Two-dimensional subaqueous dune dynamics under unidirectional flows

A. Valance, *Institut de Physique de Rennes, CNRS, Université de Rennes, Rennes, France – alexandre.valance@univ-rennes1.fr*
S. Kiki, *Institut de Physique de Rennes, CNRS, Université de Rennes, Rennes, France*
N. Le Dantec, *Laboratoire Géoscience Océan, Institut Universitaire Européen de la Mer, Plouzané, France*

ABSTRACT: Two-dimensional subaqueous dunes under the shearing of a turbulent flow are investigated experimentally and theoretically. Experiments reveal the existence of steady-state dunes migrating with constant speed. We identified two different morphological regimes. For small dune, the height of the dune varies almost linearly with its mass. In contrast, for large dune, the height and length scale as the square root of the dune mass resulting in a scale invariant dune shape. Adapting aeolian dune models based on the concept of the saturation length to subaqueous sediment transport, we derive theoretical predictions that are in quantitative agreement with our experimental data and allow to infer the saturation length from the experiments.

1 INTRODUCTION

Dunes are sedimentary bodies widely spread in Earth environments. They are found in sand deserts as well as in sea floors. An interesting feature of dunes is that their morphologies provide pieces of information about climatic conditions since they are modeled by ambient streams (Partelli et al. 2014, Courrech du Pont 2015).

Since the pioneer work of Bagnold (1941) on dune morphogenesis, it is known that dunes are generated by aerodynamic or hydrodynamic instability which amplifies any surface irregularities of a granular bed due to a phase shift between the basal shear stress and the bed topography (Sauerman et al 2001, Charru & Mouilleron-Arnoud 2002). This destabilizing mechanism is however balanced on one hand by the gravity force which tends to settle particles and on the other hand by the sediment transport dynamics. Several models for dune formation (Kroy et al 2022, Andreotti et al. 2002 b, Charru et al 2006) have indeed emphasized that the transport dynamics react to a local change of the basal fluid shear stress with a finite spatial lag, often referred to as the saturation length. This saturation process introduces a stabilizing mechanism for dune growth and sets the wavelength of the most unstable wavelength.

One important issue is to determine the relevant physical mechanisms that govern this saturation process. This leads to controversial propositions for the saturation during the last decades. Assuming the balance between particle inertia and fluid drag force dominates the dynamics of particle transport, Andreotti et al. (2002b) suggested that the saturation length is governed by the drag length which corresponds to the distance needed for a particle initially at rest to reach the fluid velocity. This hypothesis has been validated for aeolian sand dune on Earth and Mars (Claudin & Andreotti 2006). Alternative mechanisms have been proposed for subaqueous transport. In particular, Lajeunesse et al. (2006) suggested that the saturation length is set by the deposition length which corresponds to the length travelled by a mobile particle before being trapped by the bed. More recently, Pähtz et al. (2013, 2014) proposed a general theoretical expression for the saturation length that takes into account the relaxation of the fluid and particle speed and particle concentration.

Recent models of dune morphogenesis are based on particle transport description that accounts for this relaxation process via the introduction of a saturation length. These models show that there exists a minimum dune size set by the saturation length and revealed different morphologies for small (i.e., of order the saturation length) and large (i.e., much larger than the saturation length) dunes (Kroy et al, 2002, Andreotti et al. 2002b). Small dunes, sometimes called smooth heaps, domes or proto-dunes are weakly asymmetric and do not exhibit slip face. Large dunes are characterized by asymmetric profiles with well-developed slip face and scale invariant shapes.

These model predictions have been derived for aeolian sand dune. It turns out that the latter model can be easily adapted for investigating subaqueous dunes. This is confirmed by the 2D dune experiments conducted by Groh et al. (2008, 2009) for testing the model of Kroy et al. (2002) developed for aeolian sand dunes. They found a fairly good qualitative agreement between their experimental results and the prediction of the model concerning the migration speed of the steady-state dune. In particular, they confirmed that the migration speed scales like the square root of the dune mass. However, no attempt has been made for a quantitative comparison between the morphological features (height, length, aspect ratio) of the experimental dunes and model predictions.

Several questions arise for the case of subaqueous dunes. Are the models developed for aeolian dunes relevant for describing subaqueous dunes? Do the models have the capability to provide predictions in quantitative agreement with the experimental results? Are the model predictions sensitive to the nature of the transport law? What is the experimental saturation length for subaqueous particle transport? The objective of this study is to provide a detailed picture of steady-state subaqueous dunes both experimentally and theoretically.

Thanks to dune experiments achieved in a quasi-two-dimensional flume, we investigated single steady-state dunes and characterize their shape and migration speed as a function of their size and flow strength. In addition, we adapted the aeolian dune models to describe subaqueous dunes and computed steady-state dune profiles. Finally, we propose a method to assess experimentally the saturation length from a comparison with model predictions.

2 EXPERIMENTS

In this section, we present our experimental results. We first describe our experimental set-up and then present the main morphological and kinematic features of steady dunes according to their size and flow strength.

2.1 Set-up

The subaqueous dune experiments are conducted in a closed channel inspired from that of Groh et al. 2008 (see Figure 1). The channel is composed by two 900 mm long rectilinear sections closed by semi-circular junctions. The cross-section of the channel is a 90mm×90mm except for the forefront rectilinear section where the width is reduced to 6 mm. The dunes are formed and observed within the narrow section. This allows to consider that the dunes are two-dimensional.

The flow is set by a propeller which is installed in the large section of the channel. We thus have a flow driven by pressure gradient with no free surface. In the configuration we investigated so far, the flow in the narrow section is fully turbulent. We checked by particle image velocimetry that the flow close to the bottom wall obeys a classical logarithmic profile:

$$U(z) = \frac{u^*}{\kappa} \ln\left(\frac{z}{z_0}\right) \quad (1)$$

where $\kappa \approx 0.41$ is the Von Kármán constant, u_0* is the wall friction velocity and z_0 the hydrodynamic roughness.

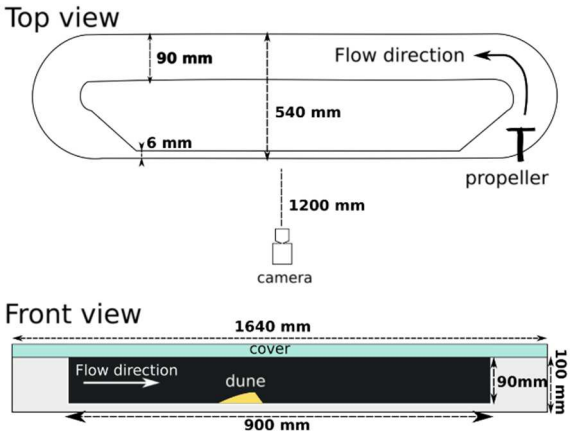

Figure 1. Scheme of the flume (top and front view).

Thanks to the determination of the flow profile throughout the whole height, it is possible to find a relationship between the friction velocity u_0* and the depth-averaged velocity $\langle U_0 \rangle$. We find $u_0^* \approx 0.064 \langle U_0 \rangle$. The strength of the flow is controlled by the propeller rotation rate.

The granular material used for the dunes are spherical glass beads with a median diameter d = 0.4 mm and a bulk density ρ_p = 2500 kg/ m^3. These particles are entrained by the flow when the latter exceeds a mean velocity $\langle U_{0c} \rangle \approx$ 0.336 m/s, which corresponds to a critical friction velocity $u_c^* \approx 0.0215$ and a critical Shields number $S_c \approx 0.08$, as summarized in Table 1.

Table 1: Critical values for incipient motion

d (mm)	$\langle U_{0c} \rangle$ (m/s)	u_c^* (m/s)	S_c
0.4	0.336	0.021	0.08

An experimental run consists of the following steps. First, the channel is filled with water before introducing a given mass m_0 of glass beads in the narrow part of the channel. The initial pile has a triangular shape and its surface area A_0 is proportional to its mass m_0: $A_0 \approx (113 \text{mm}^2/\text{g}) \times m_0$. Once the pile is formed, the propeller is turned on to the desired rotation rate and the dune morphodynamics is documented via a Nikon D610 Reflex camera with a resolution of 6016 × 4016 pixels. The spatial resolution is 0.12 mm per pixel and the images are captured with a rate of one image per second.

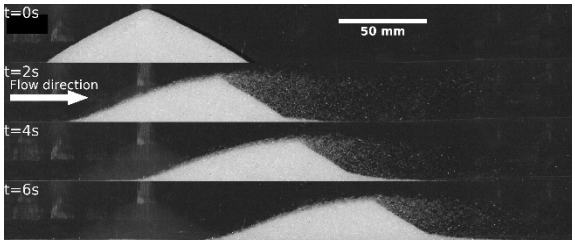

Figure 2. Successive snapshots illustrating the morphodynamics of a dune starting from an initial triangle shape. Experimental parameters: m_0 = 15 g, $\langle U_0 \rangle \approx$ 0.43 m/s.

From the captured images (see Fig. 2), we can extract the dune profile by a classic method thanks to the contrast between the dune and the dark background. We can thus easily document the temporal evolution of the height H, length L, area A and position of the dune. On the example illustrated in Fig. 2, we observe that the height, length and area of the dune reach after a very short transient (less than 1s) stationary values. Similarly, the migration speed of the dune is quickly stabilized..

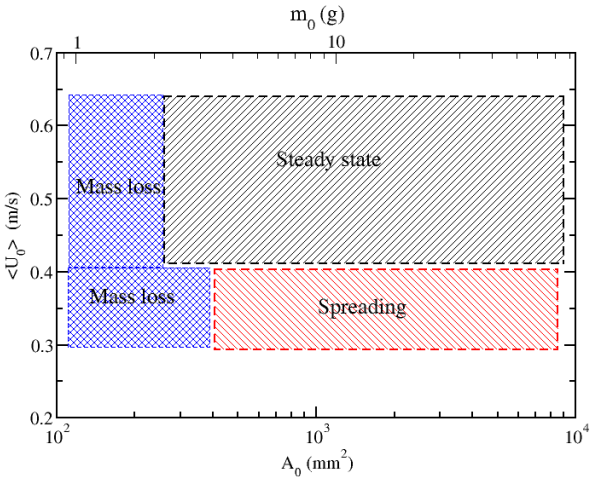

Figure 3. Regime map in the diagram ($\langle U0 \rangle$, A_0): Three scenarios are observed including spreading, steady state and mass loss.

We investigate a range of dune mass from 2 to 50g and a range of mean flow velocity from 0.3 to 0.55m/s (i.e., $0.8 < S_0/S_c < 3.5$). We identify three different regimes: (i) a spreading regime, (ii) a steady-state regime and (iii) a regime with mass loss. The observed behaviors are reported in the phase diagram $\langle U_0 \rangle$ versus A_0 (see Fig. 3). For flow velocities ranging from 0.4m/s to

0.65m/s (i.e., $1.5<S_0/S_c<3.5$) and dune mass $m_0>2g$, the dune reaches a steady-state where its shape becomes stationary and its migration speed constant. In the following, we will document essentially the steady-state regime and disregard the other regimes.

2.2 Height, length and aspect ratio of the steady dune

The variation of the height H, length L and aspect ratio R=H/L of steady-state dunes exhibit two different behaviors according to the dune size (see Fig. 4). For small dunes (i.e., $A_0<1000$ mm^2), H, L and R can be locally described by scaling laws as a function of the dune area A_0:

$$\frac{H}{d} = K_H \left(\frac{A_0}{d^2}\right)^{\alpha} \qquad (2)$$

$$\frac{L}{d} = K_L \left(\frac{A_0}{d^2}\right)^{\beta} \qquad (3)$$

$$R = K_R \left(\frac{A_0}{d^2}\right)^{\gamma} \qquad (4)$$

with $\gamma=\beta-\alpha$. The scaling exponents α and β exhibit a weak dependence with the dune size: α decreases progressively from 0.85 down to 0.5 with increasing dune size while and β increases from 0.35 up to 0.5. In contrast, for large dunes (i.e., A_0 >1000 mm^2), the scaling exponents do not show any variation and we get: $\alpha = \beta = 0.5$ and $\gamma=0$. This regime corresponds to the asymptotically large dune regime where the aspect ratio is invariant. The coefficients K_H, K_L and K_R appearing in the scaling laws are found to increase slightly with increasing flow strength.

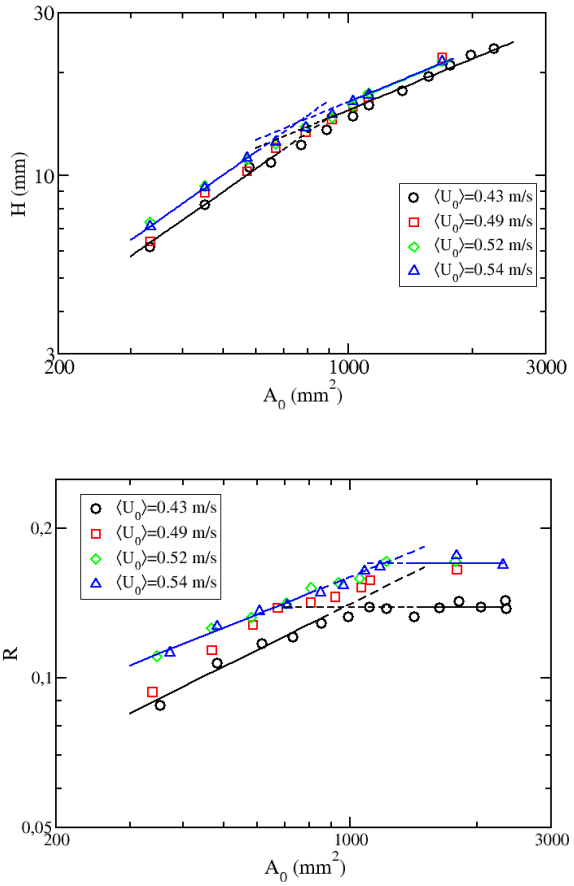

Figure 4: Height H and aspect ratio R of the steady dune as a function of the dune area for different flow strengths (< U_0 >=0.43,0.49,0.52 and 0.54 m/s).

2.3 Dune shape

Fig. 5a presents the profiles of steady-state dune at a given flow strength (<U_0>≈ 0.43 m/s and S_0/S_c= 1.6) for various dune mass ranging from 2g to 20g. Except for the smallest dune (m_0=2g), the dune profiles are asymmetric with a well-developed slip face in the downstream side. The local slopes associated to the dune profiles are shown in Fig. 5b. We observe an increase of the slope with increasing dune size both on upstream and downstream faces. The maximum slope of the upstream and downstream faces increases with increasing dune size in the small dune regime and saturates in the large dune regime to a value of 17° and 35°, respectively. These asymptotic values increase with increasing flow strength. For the largest flow strength, we investigate (S_0/S_c=2.4), the maximum slope on the upstream and downstream face are 20° and

40°, respectively. The strength of the flow has thus a non-negligible effect of the angle of the downstream slip face.

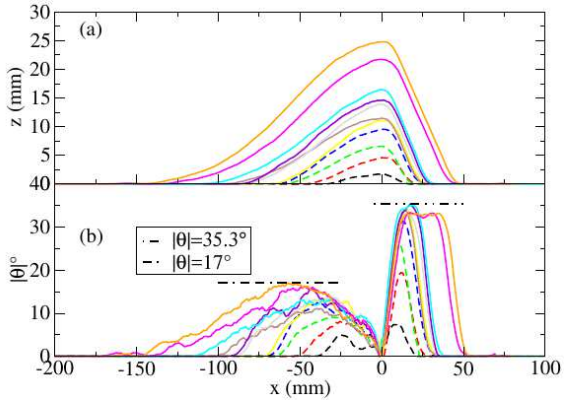

Figure 5: Profiles of steady-state dunes for a given flow strength $\langle U_0 \rangle \approx$ 0.43m/s (S_0/S_c= 1.6): From the bottom to the top, the mass m_0 are respectively 2, 3, 4, 5, 6, 7, 8, 9, 10, 16 and 20g. (b) Local slopes of the steady-state profiles.

Fig. 6 shows the dune profiles rescaled in both direction by their length L. This figure illustrates the gradual transition to the large dune regime which is scale invariant.

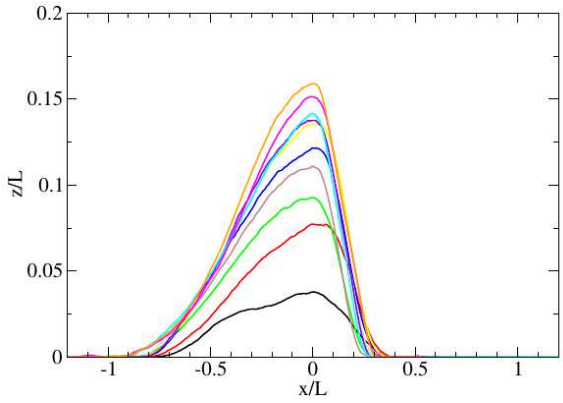

Figure 6: profiles of steady-state dune rescaled by their length L in both directions. From the bottom to the top, the mass m_0 are respectively 2, 3, 4, 5, 6, 7, 8, 9, 10, 16 and 20g. Experimental parameters: $\langle U_0 \rangle \approx$ 0.43 m/s.

2.4 Migration speed

The migration speed of steady-state dunes as a function of the dune size is shown in Fig. 7a for different flow strengths. It decreases with increasing dune size and increases with increasing flow strength as expected. We observe a single scaling regime for small and large dunes:

$$\frac{V}{[(s-1)gd]^{\frac{1}{2}}} = K_v \left(\frac{A_0}{d^2}\right)^{-\frac{1}{2}} \qquad (5)$$

where $s=\rho_p/\rho_{fluid}$. The scaling exponent is −1/2, which is in agreement with the observations by Groh et al. (2008, 2009) for subaqueous dunes. This result is also consistent with the prediction of the dune model for large dune regime.

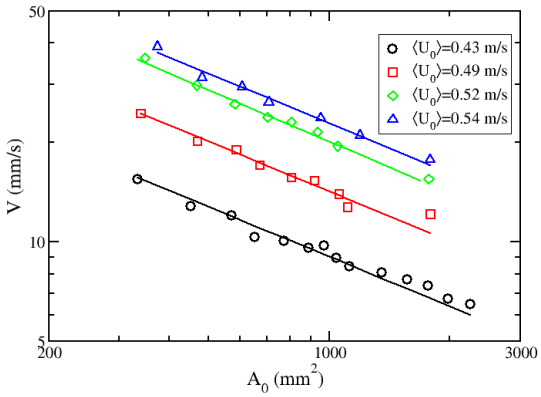

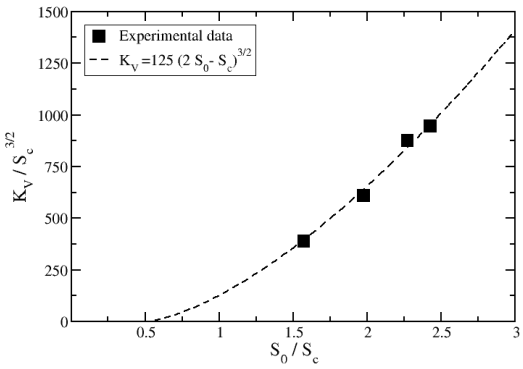

Figure 7: (a) Migration speed of the steady dune as a function of the dune area for different flow strengths. (b) Coefficient K_v (see eq. 5) as a function of the Shields number S_0.

The coefficient K_V which encodes the influence of the flow strength is shown in Fig. 7b and is found to obey the following power law:

$$K_v = K_{v0}(2S_0 - S_c)^{\frac{3}{2}} \qquad (6)$$

K_V is linked to the mass flux Q_{crest} at the top of the dune. In the large dune regime, the latter can be easily calculated:

$$Q_{crest} = V \times H = K_v \times K_H = 65\, Q_0 (2S_0 - S_c)^{\frac{3}{2}} \qquad (7)$$

We recall that the law of Meyer-Peter and Müller for the saturated flux is given by $Q_{MPM}=8Q_0\ (S_0 - S_c\ )^{3/2}$. We thus find a law similar to that of Meyer-Peter and Müller with a 3/2 exponent. The factor 2 which multiplies the Shields number can be interpreted as the shear stress increase factor at the top of the dune. This value is in agreement with the measurements by Charru & Franklin (2012). We can note that the proportionally factor in Eq. (7) is much higher than that in the law of Meyer-Peter and Müller flow (65 against 8).

3 THEORETICAL MODELING

We used the theoretical continuum model developed by Kroy et al.(2002) for aeolian sand dunes and adapted it to the situation of subaqueous dunes. The model is explained in details in S. Kiki (2019). We recall here briefly the main assumptions of the model.

3.1 Model equation

The equation describing the temporal evolution of a sand heap on a flat and horizontal substrate subject to the shearing of a turbulent flow is inferred from mass conservation and reads:

$$\frac{\partial h(x,t)}{\partial t} = -\frac{1}{\rho_b}\frac{\partial Q(x,t)}{\partial x} \qquad (8)$$

where h(x, t) and Q(x,t) are the local height and mass flux, respectively, at position x and time t. ρ_b is the bulk density of the dune. We assume that the mass flux Q_{sat} at saturation (or equilibrium) is given by the empirical formulation of Meyer-Peter and Müller (1948) :

$$Q_{sat} = Q_{MPM} = 8Q_0(S(x,t) - S_c)^{\frac{3}{2}} \quad (9)$$

For unsteady or non-uniform conditions, the particle flux is not necessarily equal to the saturated flux because the relaxation towards the saturated value is not instantaneous. For non-uniform flow conditions, the case we are interested in, the relaxation process can be simply modeled by (Andreotti et al., 2002b, 2010, Valance et al., 2005a,b):

$$\frac{\partial Q(x,t)}{\partial x} = \frac{Q(x,t) - Q_{sat}(x,t)}{l_{sat}} \qquad (10)$$

where l_{sat} is the saturation length and sets the characteristic length scale for the relaxation process. To compute the saturated flux at any position along the dune profile, it is necessary to assess the local fluid shear stress τ at the bed. To do this, we employ the approximated formulation of Jackson et al. (1975) which reads:

$$\frac{\tau(x,t)}{\tau_0} = 1 + A\int_{-\infty}^{+\infty} \frac{dx'}{\pi x'}\frac{\partial h}{\partial x}(x - x') + B\,\frac{\partial h}{\partial x}(x) \qquad (11)$$

where τ_0 is the unperturbed fluid shear stress upstream the dune (note that $\tau/\tau_0=S/S_0$). We define the corresponding Shields number $S_0=\tau_0/(\rho_p-\rho_{fluid}\ )gd$, which characterizes the basal shear stress in the absence of dune. Eq. (11) is valid in the limit of small relief, that is $H/L << 1$. $\mathcal{A}$ and $\mathcal{B}$ are parameters which depend logarithmically on the dune size. More specifically, they depend on the relative roughness of the dune z_0/L where z_0 is the hydrodynamical roughness of the sand bed surface. If the range of variation of the ratio z_0/L is limited to one decade, $\mathcal{A}$ and $\mathcal{B}$ can be fairly considered as constant parameters. For our purpose, we will use two sets of parameters ($\mathcal{A}$, $\mathcal{B}$): (4.2, 2) and (4.2, 3.8) (see Kiki 2019). The first set is obtained from a simple turbulent model based on the Prandtl turbulent length and the second one from a more elaborated turbulent model (Frederick & Hanratty 1988). For calculating both sets of values, we took $L/z_0 \sim 10^4$ which corresponds to our experimental conditions. Note that for terrestrial aeolian dune, $\mathcal{A}$ and $\mathcal{B}$ are slightly different: $\mathcal{A}$ = 4 and $\mathcal{B}$ = 1.

Eqs. (8-11) form a close set of equations for the dune morphodynamics. This description is very similar to that developed by Kroy et al (2002). However, we should emphasize that we disregard two mechanisms that are included in the original model: i) the phenomenon of flow separation and ii) the avalanche process at the lee side. These mechanisms have been recognized to be important for a detailed description of the equilibrium dune shape. However, we have shown (Kiki, 2019) that those are in fact of secondary importance for predicting the height, length and migration speed of equilibrium dune shape.

3.2 Model predictions

The model reveals the existence of three distinct regimes: an asymptotical small and large dune regime, and a cross-over regime. The asymptotical small dune regime is characterized by a linear increase of the equilibrium height and aspect ratio as a function of the dune area:

$$H = \frac{2A_0}{\lambda_c} \; and \; R = \frac{2A_0}{\lambda_c^2} \quad (12)$$

where λ_c is the cut-off wavelength deduced from the linear stability analysis of a flat bed ($\lambda_c = (2\pi\mathcal{A}/\mathcal{B})l_{sat}$). The small regime is observed for $A_0 < 3\ l_{sat}^2$. In contrast, in the asymptotical large dune regime ($A_0 > 100\ l_{sat}^2$), the height varies as the square root of the dune area whereas the aspect ratio is invariant:

$$H = K_H^{\infty} A_0^{\frac{1}{2}} \; and \; R = \frac{K_H^{\infty 2}}{2} \quad (13)$$

The proportionality coefficient K_H^{∞} depends on $\mathcal{A}$, $\mathcal{B}$ and S_0/S_c but not on l_{sat}. The transition or cross-over regime occurs for intermediate dune sizes ($3\ l_{sat}^2 < A_0 < 100\ l_{sat}^2$) as shown in Fig. 9.

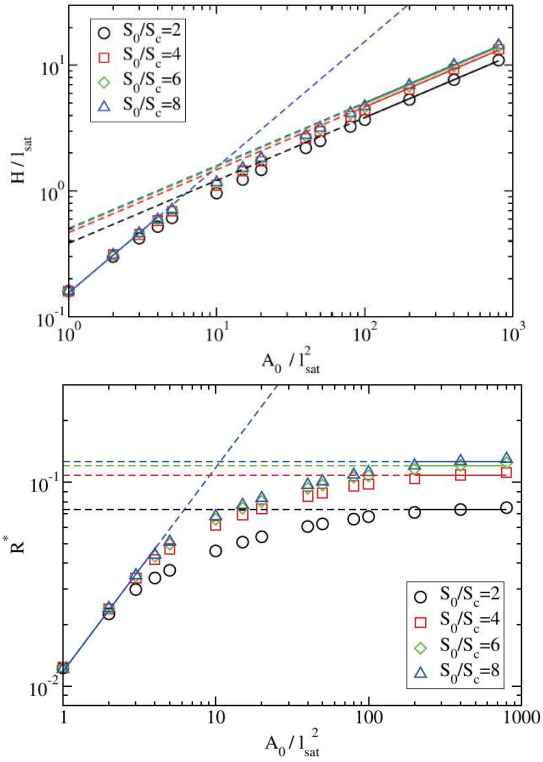

Figure 8: Height (a) and aspect ratio (b) of steady dune as a function of the dune size for different flow strengths. Model parameters: $\mathcal{A}$=4.2 and $\mathcal{B}$=2.

3.3 Discussion

The large dune regime observed in the experiments do correspond to the asymptotically large dune regime of the model. In contrast, the small dune regime identified in the experiments do not match with the asymptotically small dune regime of the model but corresponds to the crossover regime between the two asymptotical regimes. A detailed comparison of the model with the experiments in the asymptotically large dune indicate that the relevant values for the model parameters are: $\mathcal{A}$=4.2 and $\mathcal{B}$=3.8 (i.e., those corresponding from the model of Frederick & Hanratty 1988). Comparison made in the cross-over regime allows to determine the saturation length l_{sat}. The procedure is explained in details in S. Kiki 2018.

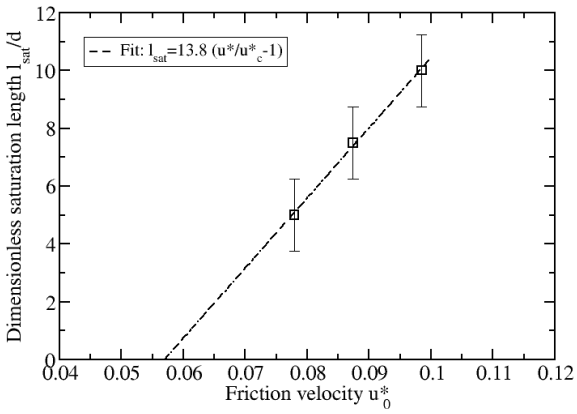

Figure 9: saturation length l_{sat} as a function u_0* inferred from comparison between experiments and model predictions.

One way to do this is to determine the value of l_{sat} which gives the best agreement between the experimental equilibrium heights and those predicted by the model for a given ratio S_0/S_c. The same procedure can be carried out with the length of the dune or aspect ratio. The outcome of these adjustments suggests that the saturation length increases with the strength of the flow. We go from 2mm for S_0/S_c=1.6 to 4 mm for S_0/S_c=2.5. This evolution seems to follow a linear law with the friction velocity u_0*.

These results also indicate a proportionality between l_{sat} and the friction velocity u_0*:

$$\frac{l_{sat}}{d} = \frac{53}{\left((s-1)gd\right)^{\frac{1}{2}}}(u_0* - u_c*) \quad (14)$$

which is compatible with a saturation length governed by a deposition length as proposed by Lajeunesse et al. (2010).

4 CONCLUSIONS

We have investigated steady-state subaqueous sand dune experimentally and theoretically. The proposed model predicts the existence of two asymptotic regimes for small and large dunes, as suggested by previous models and a cross-over regime for intermediate dune sizes. In the small dune regime, the dune length is set by the saturation length and the dune height scales linearly with the dune mass. In the large dune regime, the dune profile is scale invariant: both height and length of the dune increases as the square root of the dune mass. Experiments confirm the existence of different regimes. We indeed identified clearly the cross-over regime and the large dune regime where the dune profile is scaling invariant. The cross-over regime teaches us about the scale of the saturation length. A comparison between experimental and theoretical dune profiles in this regime allowed us to assess the experimental saturation length. Our results suggest that the saturation length is governed by the deposition length rather the drag length.

5 REFERENCES

Andreotti, B., and Claudin, P. (2002). The European Physical Journal B 28, 341.

Andreotti, B., Claudin, P., and Douady, S. (2002). The European Physical Journal B 28, 321.

Bagnold, R. A. (1941). The physics of blown sand and desert dunes. London: Methuen.

Charru, F. (2006). Selection of the ripple length on a granular bed sheared by a liquid flow. Physics of fluids 18, 121508.

Courrech Dupont, S. (2015). Dune morphodynamics. Comptes Rendus Physique 16, 118.

Groh, C., Wierschem, A., Aksel, N., Rehberg, I., and Kruelle, A.C. (2008). Barchan dunes in two dimensions: Experimental tests for minimal models. Phys. Rev. E 78, 021304.

Groh, C., Rehberg, I., and Kruelle, A.C. (2009). How attractive is a barchan dune. New J. Phys. **11** 023014.

Jackson, P. S, and Hunt, J. C. R (1975). Turbulent Wind Flow over a Low Hill. Quart. J. R. Met. Soc. 101, 929.

Kiki, S, 2018. Caractérisation de la morphologie des dunes aquatiques dans des écoulements unidirectionnels et alternatifs. PhD Thesis. University of Rennes.

Kroy, K., Sauermann, G., and H. J. Herrmann, H.J. (2002). Minimal model for aeolian sand dunes. Phys. Rev. E 66, 031302.

Lajeunesse, E., Malverti, L. and Charru, F. (2010). Bed load transport in turbulent flow at the grain scale: Experiments and modeling . Journal of Geophysical Research: Earth Surface 115, 2003–2012.

Meyer-Peter, E. and Müller, R. (1948). Formula for the bedload transport. Proceedings of the 3rd Meeting of the International Association of Hydraulic Research.

Parteli, E.J., Durán, O., Bourke, M. C., Tsoar H., Pöschel, T. and Herrmann, H. (2014). Origins of barchan dune asymmetry: Insights from numerical simulations. Aeolian Research 12, 121.

Sauermann, G., Kroy, K. and Herrmann, H.J (2001). Continuum saltation model for sand dunes. Phys. Rev. E 64, 031305.

Valance, A. and Langlois, V. (2005). Ripple formation over a sand bed submitted to a laminar shear flow. Eur. Phys. J. B 43, 283–294.

Valance, A. (2005). Ripple formation over a sand bed submitted to a turbulent shear flow. Eur. Phys. J. B 45, 433–442.